Importance of quantum correction for the quantitative simulation of photoexcited scanning tunneling spectra of semiconductor surfaces

M. Schnedler, R. E. Dunin-Borkowski, and Ph. Ebert

Peter Grünberg Institut, Forschungszentrum Jülich GmbH, 52425 Jülich, Germany

(Received 4 March 2016; revised manuscript received 3 May 2016; published 31 May 2016)

Photoexcited scanning tunneling spectroscopy is a promising technique for the determination of carrier concentrations, surface photovoltages, and potentials of semiconductors with atomic spatial resolution. However, extraction of the desired quantities requires computation of the electrostatic potential induced by the proximity of the tip and the tunnel current. This calculation is based on an accurate solution of the Poisson as well as the continuity equations for the tip-vacuum-semiconductor system. For this purpose, the carrier current densities are modeled by classical drift and diffusion equations. However, for small tip radii and highly doped materials, the drift and diffusion transport model significantly overestimates a semiconductor's carrier concentration near the surface, making the quantification of physical properties impossible. In this paper, we apply quantum correction to the drift and diffusion model, in order to account for the so-called quantum compressibility, i.e., reduced compressibility of the carrier gas due to the Pauli principle, in the region of the tip-induced band bending. We compare carrier concentrations, potentials, and tunnel currents derived with and without quantum correction for GaN($10\bar{1}0$) and GaAs(110) surfaces to demonstrate its necessity.

I. INTRODUCTION

Photoexcited scanning tunneling spectroscopy (STS) is a powerful tool for the investigation of illumination-induced local surface photovoltage, band bending, carrier concentration, electrostatic potential distribution, and transport parameters with atomic spatial resolution [1–10]. However, the extraction of these physical quantities from photoexcited STS usually requires quantitative simulations [9,11–16]. Recently, we presented a quantitative description of photoexcited STS and applied it to photoexcited spectra measured from *p*-doped nonpolar GaAs(110) surfaces [10]. The potential and charge carrier distributions of the tip-vacuum-semiconductor system were calculated using the Poisson equation and the continuity equations for electrons and holes. The carrier current density is given by the classical drift and diffusion transport model. A Scharfetter-Gummel discretization and a three-dimensional finite difference algorithm were applied to solve this system of coupled differential equations [10,17,18].

Although classical drift and diffusion equations are valid in most regions of a semiconductor, significantly overestimated carrier concentrations may be obtained in the tip-induced band bending region for tips with small apex radii and semiconductors with high doping concentrations: in this strongly confined region near the semiconductor surface (so-called *tip-induced quantum dot*) the classical drift and diffusion transport model does not account for the reduced compressibility of an ideal quantum gas [19] (i.e., the *quantum compressibility* [20]). Since an overestimation of the carrier concentration has a major impact on the extraction of nearly all other physical properties, there is a need to extend the classical drift and diffusion transport model to include quantum compressibility. Here, the impact of this *quantum correction* on the extraction of physical properties is illustrated exemplary for ground state and photoexcited tunneling spectra on GaN($10\bar{1}0$) and GaAs(110) surfaces, respectively.

II. QUANTUM COMPRESSIBILITY

Based on the Pauli principle, it is well known that two electrons at the same place cannot occupy the same quantum state. This is a fundamental concept of quantum mechanics and must also be considered in the description of free electron gases. It induces a repulsion between electrons (or holes) and hence limits the compressibility of the electron (hole) gas [20]. Such quantum mechanical effects become important for device feature sizes or quantum dot sizes on the order of the de Broglie wavelength [21], which is, e.g., approximately 17 nm for electrons in GaAs at room temperature. As this criterion is fulfilled for quantum dots induced by sharp tips (i.e., tip radius in the order of the de Broglie wavelength) and moderate doping concentrations (i.e., free carrier concentration $\gtrsim 10^{18}$ cm^{-3}), the application of a simple classical drift and diffusion transport model will overestimate the carrier densities in this region. Although many widely used device simulators still rely on this classical treatment, a variety of different strategies [22,23] have been developed in recent years, including a quantum mechanical description of the semiconductor device modeling. Particularly noteworthy is a density-gradient model derived by Ancona and Tiersten [24]. In this paper we apply a slightly different approach that is especially suited for the description of high carrier concentrations inside a tip-induced quantum dot. The idea is to extend the recently derived model for the quantitative simulation of photoexcited STS [10] in order to account for quantum compressibility.

III. REFINEMENT OF THEORETICAL MODEL IN THERMAL EQUILIBRIUM

In the drift and diffusion equations [Eqs. (8) and (9) in Ref. [10]] the Einstein relation connects the mobility and diffusivity of electrons and holes in the semiconductor. Since the Einstein relation is based on Maxwell-Boltzmann statistics, the accuracy of the drift and diffusion equation also depends

on their validity [21]. Although Maxwell-Boltzmann statistics usually hold for low and medium doped semiconductors ($\lesssim 1 \times 10^{18}$ cm^{-3}) [25], the carrier concentration inside the tip-induced quantum dot may be far above the limit of validity for this distribution function. Hence Maxwell-Boltzmann statistics have to be replaced by Fermi-Dirac statistics in the Einstein relation [26]. Following the idea of Pinto [26] and Rowsey *et al.* [21] we define perturbation factors γ_n and γ_p that account for the deviation between the electron and hole concentrations n_MB and p_MB derived using the Maxwell-Boltzmann distribution function and the concentrations n_FD and p_FD obtained employing the Fermi-Dirac distribution function:

$$\gamma_\text{n} := \frac{n_\text{FD}}{n_\text{MB}} = F_{\frac{1}{2}}\left(\frac{E_\text{F} - E_\text{C}}{kT}\right) \exp\left(\frac{E_\text{C} - E_\text{F}}{kT}\right), \quad (1)$$

$$\gamma_\text{p} := \frac{p_\text{FD}}{p_\text{MB}} = F_{\frac{1}{2}}\left(\frac{E_\text{V} - E_\text{F}}{kT}\right) \exp\left(\frac{E_\text{F} - E_\text{V}}{kT}\right). \quad (2)$$

E_V (E_C) denotes the valence (conduction) band edge, $F_{\frac{1}{2}}$ is the Fermi-Dirac integral, and E_F denotes the Fermi energy in thermal equilibrium. With the help of the definitions (1) and (2), the carrier concentrations derived using Fermi Dirac statistics can be rewritten as follows:

$$n_\text{FD} = \gamma_\text{n} \times n_\text{MB} = \gamma_\text{n} N_\text{C} \exp\frac{E_\text{F} - E_\text{C}}{kT}, \quad (3)$$

$$p_\text{FD} = \gamma_\text{p} \times p_\text{MB} = \gamma_\text{p} N_\text{V} \exp\frac{E_\text{V} - E_\text{F}}{kT}, \quad (4)$$

where N_V and N_C are the effective densities of states of the valence and conduction band, respectively (as, e.g., defined in Ref. [10]). The right hand side of Eqs. (3) and (4) can be mathematically transformed such that the perturbation factors appear in the argument of the exponential function only. This allows for the introduction of additional repulsive potentials $\phi_\text{n,rep}$ and $\phi_\text{p,rep}$ that prevent further compression of the carrier gases, when described by Maxwell-Boltzmann statistics [21]:

$$n_\text{FD} = N_\text{C} \exp\frac{E_\text{F} - E_\text{C} + kT \ln \gamma_\text{n}}{kT}$$
$$= N_\text{C} \exp\frac{E_\text{F} - E_\text{C} + e\phi_\text{n,rep}}{kT}, \quad (5)$$

$$p_\text{FD} = N_\text{V} \exp\frac{E_\text{V} - E_\text{F} + kT \ln \gamma_\text{p}}{kT}$$
$$= N_\text{V} \exp\frac{E_\text{V} - E_\text{F} - e\phi_\text{p,rep}}{kT}. \quad (6)$$

The repulsive potentials $\phi_\text{n,rep}$ and $\phi_\text{p,rep}$ are thus defined as

$$\phi_\text{n,rep} := \frac{kT}{e} \ln \gamma_\text{n}, \quad (7)$$

$$\phi_\text{p,rep} := -\frac{kT}{e} \ln \gamma_\text{p}. \quad (8)$$

According to Eqs. (1), (2), (7), and (8) they tend to zero for semiconductor regions, where no quantum correction, i.e., correction for quantum compressibility, is required, since in these regions Maxwell-Boltzmann statistics equal Fermi-Dirac statistics. Equations (7) and (8) are suitable for application in the numerical iteration scheme presented in Ref. [10]:

at the beginning of every Newton iteration step, $\phi_\text{n,rep}$ is derived from the electron concentration $n_\text{i,j,k}$, known from the previous iteration step, for every node point (i,j,k) of the semiconductor. The sum $\phi_\text{i,j,k} + \phi_\text{n,rep}$ then replaces the potential $\phi_\text{i,j,k}$ in the iteration formula for the electron concentration [Eq. (12) in Ref. [10]]. The iteration formula for the hole concentration is modified analogously.

IV. QUANTUM COMPRESSIBILITY FOR EXCITED SEMICONDUCTORS

At this stage, we focus on the quantum compressibility of the carrier gases in photoexcited semiconductors. Under illumination, electron-hole pairs are generated in the semiconductor. In order to account for these excited carriers in all of the equations presented above [i.e., Eqs. (1)–(8)], the Fermi energy E_F has to be replaced by quasi-Fermi energies $E_\text{FQ,V}$ and $E_\text{FQ,C}$ for holes and electrons, respectively (see, e.g., Ref. [10]).

The quasi-Fermi energies are required for the calculation of the perturbation factors γ_n and γ_p, as well as for the computation of the tunnel current (cf. Sec. IV B in Ref. [10]) and the surface charge density (cf. Sec. V C in Ref. [10]). Calculations incorporating quantum compressibility reveal significantly reduced carrier concentrations in the region of the tip-induced quantum dot. Thus, instead of deriving the quasi-Fermi levels by integrating over the density of states [10] obtained from theoretical computations to account for high carrier concentrations, it is now sufficient to assume parabolic bands. Remaining within the framework of the parabolic band approximation has several advantages: first, one can use analytical approximations for the inverse Fermi-Dirac integral, such as the inverse Joyce-Dixon approximation [27], to speed up the iteration. Second, instead of depending on the full band structure, $E_\text{FQ,V}$ and $E_\text{FQ,C}$ are evaluated with the help of effective density of states masses. While the effective masses are known explicitly, we find significant differences, e.g., between the density of states of GaAs calculated by Chelikowsky and Cohen [28,29] and that presented by, e.g., Yin *et al.* [30]. The results of Chelikowsky and Cohen were used in Ref. [10] and likely overestimate the density of states near the conduction band edge. Such deviations of the density of states, particularly at the band edges, critically affect quasi-Fermi energies and thus tunnel currents.

In view of the initial objective of the extraction of physical quantities (i.e., surface photovoltage, carrier concentrations, potentials, transport parameters) from photoexcited STS, much more accurate results should be obtained by applying the quantum correction and the parabolic band approximation, as a result of a reduction in carrier concentrations.

V. RESULTS OF CALCULATION

In order to illustrate the importance of the preceding discussion, we compare the results of tunnel current simulations with and without taking into account quantum compressibility.

A. GaN(10$\bar{1}$0)

As a first example we focus on the nonpolar *m*-plane GaN cleavage surface (free carrier concentration $\approx 3 \times 10^{18}$ cm^{-3}). A typical current voltage spectrum measured on a clean
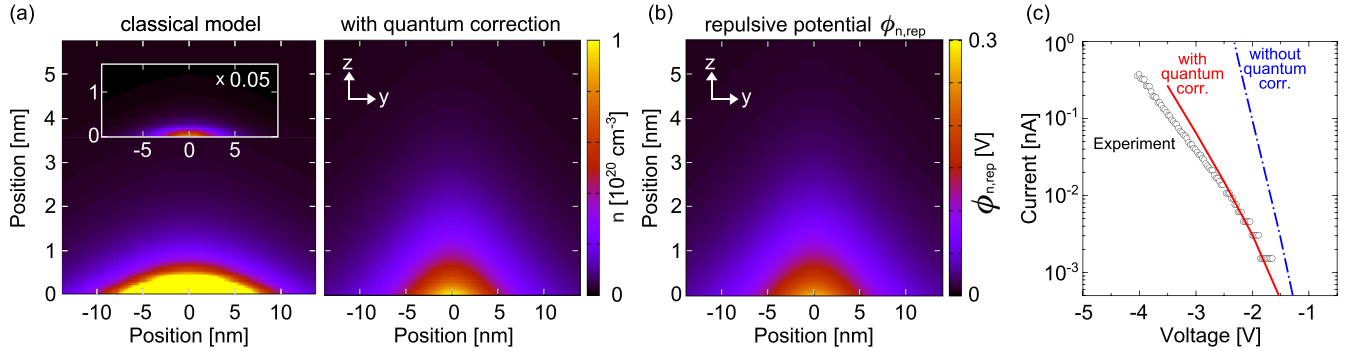
FIG. 1. (a) Calculated cross-sectional plots of the electron concentration in the tip-induced quantum dot near the $(10\bar{1}0)$ surface of a n-doped GaN for a sample voltage of -3.5 V. Left frame: electron concentration for the classical drift-diffusion model without inclusion of quantum compressibility. The actual electron concentration near the surface is much higher than the scale contrast available. Hence the inset shows the area directly at the surface scaled by a factor of 0.05 compared to the color scale. Right frame: electron concentration for a drift-diffusion model taking into account quantum compressibility. By including this quantum correction, the electron concentration decreases by approximately a factor of 20 near the surface. (b) Cross-sectional plot of the repulsive potential $\phi_{n,\text{rep.}}$. The repulsive potential reaches its maximum in the region of the tip-induced quantum dot near the surface, where the electron concentration is highest, and decreases to zero inside the semiconductor. (c) Tunnel spectrum measured on the clean, nonpolar n-doped GaN$(10\bar{1}0)$ cleavage surface (circles) taken from Ref. [16]. The red solid line corresponds to the simulation of the tunnel current with quantum correction. Onset voltage and slope of the calculated curve coincide with the measurement. In contrast the results of the same simulation without quantum correction, as shown by the blue dash-dotted line, cannot reproduce the measurement. The tunnel current is increased by at least one order of magnitude.

GaN$(10\bar{1}0)$ surface in ultrahigh vacuum and at 300 K is shown as black circles in Fig. 1(c). Since we focus on the electron accumulation near the surface, the spectrum is shown for negative sample voltages only. At positive voltages electrons cannot accumulate and hence the quantum correction does not affect the positive branches of the tunnel current spectra. For our simulations, we assume a tip radius of 10 nm and a tip-sample separation of 1.04 nm. Calculations with and without quantum correction were performed with identical parameters. In both cases, the quasi-Fermi energies were obtained by using parabolic band approximations. Hence all changes, in both carrier concentrations and tunnel currents, are a direct consequence of the quantum correction only.

Figure 1(a) shows cross-sectional plots of the electron concentration in the GaN semiconductor without (left frame) and with (right) quantum correction for -3.5 V sample voltage. One clearly observes that the peak electron density is lower by a factor of about 20 and hence the electron gas is compressed less in the latter case. The cross-sectional plot of the repulsive potential in Fig. 1(b) illustrates that $\phi_{n,\text{rep}}$ reaches its maximum ($\sim$0.3 V) in the region of the tip-induced quantum dot near the surface, where the electron concentration is highest, and decreases to zero inside the semiconductor.

The different surface electron concentrations critically affect the tunnel current, as indicated in Fig. 1(c): the red solid line corresponds to the simulation of the tunnel current with quantum correction. Onset voltage and slope of the calculated curve agree with the experimental data. In contrast the results of the same simulation without quantum correction (blue dash-dotted line) cannot reproduce the measurement: the calculated tunnel current is larger by at least one order of magnitude (small negative sample voltages) or even more (larger negative sample voltages). Hence the quantum correction significantly alters the tunnel current simulation.

B. GaAs(110)

As a second example, we recall the measurement on GaAs(110) and simulations (without accounting for quantum compressibility) presented in Ref. [10]: photoexcited STS was performed on a p-doped GaAs(110) surface, which was illuminated by a 1 mW laser diode at a wavelength of 785 nm. An increased tunnel current was observed under illumination for negative sample voltages. In contrast, at positive voltages, the tunnel current remained unchanged. We demonstrated that this effect is determined mainly by the accumulation of photoexcited electrons in the region of the tip-induced quantum dot at negative sample voltages. The question is to what extent the electron concentration in the tip-induced quantum dot will be reduced due to quantum compressibility and how this change will affect the tunnel current.

In order to answer this question, we turn to the cross-sectional plots presented in Fig. 2: the plots (a1) and (a2) show the calculated electrostatic potential of the tip-vacuum-semiconductor system for a sample voltage of -1.5 V, a tip-sample separation of 0.925 nm, and a tip radius of 20 nm [31]. The plots (b1) and (b2) show the corresponding electron concentrations. The results presented in the right column [(a2) and (b2)] are based on a simulation that includes quantum compressibility. The quasi-Fermi energies were derived in the parabolic band approximation (see Sec. IV). In contrast, the results in the left column [(a1) and (b1)] were obtained without accounting for quantum correction and by determining the quasi-Fermi energies using the density of states calculation of Chelikowsky and Cohen [28,29]. The data in the latter two plots were taken from Ref. [10]. All other input parameters of both simulations (i.e., tip-sample separation, irradiance of the laser, etc.) were the same.

A comparison of the simulations reveals a lower electron concentration in the region of the tip-induced quantum dot for the simulation that incorporates quantum compressibility. The
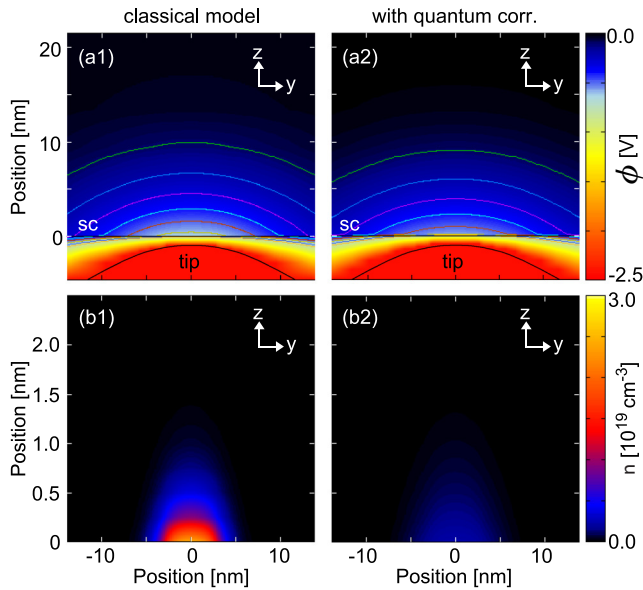
FIG. 2. Calculated cross-sectional plots of (a1),(a2) the electrostatic potential ϕ and (b1),(b2) the electron concentration n for a tip (tip radius 20 nm) located 0.925 nm away from a GaAs(110) sample surface ([Zn] = (1–2) × 10^{18} cm^{-3}) under illumination. Left column: classical results without accounting for quantum compressibility, taken from Ref. [10]; right column: results incorporating the correction for quantum compressibility. A sample voltage of −1.5 V is applied. The interface between semiconductor (SC) and vacuum is at the position $z = 0$ (vertical axes). Equipotential lines are drawn in steps of −0.1 V, starting with the green line at a potential of −0.1 V. The reduced tip-induced band bending in (a2) compared to (a1) is attributed mainly to the refined determination of the quasi-Fermi levels (compared to Ref. [10]), while the reduced electron concentration in (b2) compared to (b1) is caused by both the reduced potential and quantum compressibility.

electron concentration is reduced by a factor of ∼10. This is in analogy to the above case of GaN(10$\bar{1}$0).

Furthermore, a decreased electrostatic potential is observed. This may seem surprising at first view, since a lower electron concentration should lead to a weaker screening of the electric field between the tip and the semiconductor and hence to an increased electrostatic potential. This apparently confusing situation is clarified by drawing attention to the surface charge density. In analogy to Refs. [10,32], we model the empty C_3 (Ga-derived) surface state as a Gaussian distribution, peaking 0.33 eV above the conduction band minimum with a FWHM of 0.25 eV and assuming one state per surface cation for both simulations. The surface state is partially occupied by photoexcited electrons up to $E_{FQ,C}$ [10]. Although the electron concentration in the tip-induced quantum dot is lowered by the reduced compressibility, the quasi-Fermi level $E_{FQ,C}$ is increased slightly, since it does not depend on the density of states calculated by Chelikowsky and Cohen anymore (cf. Sec. IV). An increased quasi-Fermi level increases the charge density in the intrinsic C_3 surface state and hence leads to a stronger screening of the tip-induced potential. Thus the reduced potential of the tip-induced quantum dot is attributed mainly to the refined determination of the quasi-Fermi levels, while the reduced electron concentration

is caused by both the reduced potential and the quantum compressibility. Note, for GaN(10$\bar{1}$0), the surface state cannot be filled at negative voltages and therefore it is not influencing the band bending [16].

We now turn to the discussion of the impact of quantum compressibility on the tunnel current. Figures 3(a) and 3(b) show measured and the simulated tunnel currents without and with incorporation of quantum compressibility, respectively, for negative sample voltages. In addition to the tunnel currents measured without (black triangles) and with (red squares) illumination, four simulated currents or current contributions are plotted in both graphs: the total current under dark conditions (black solid line), the current components under illumination arising from tunneling out of the valence band (I_V, green dashed line) and out of the conduction band (I_{Photo}, blue dash-dotted line) and the total current under illumination (red solid line), which is the sum of the components I_V and I_{Photo}. For the reasons of comparability, the additional, red dotted line in Fig. 3(a) corresponds to the simulated total tunnel current of an illuminated sample without quantum correction, but incorporating the parabolic band approximation.

First, comparing the simulation of the tunnel current under dark conditions [black lines in Figs. 3(a) and 3(b)] reveals no change when introducing the quantum correction, because no electrons accumulate in the tip-induced quantum dot (minority carriers in p-type GaAs). Second, the current component arising from photoexcited electrons tunneling out of the conduction band (I_{Photo}, blue dashed-dotted lines) is reduced significantly for the quantum corrected model as compared to the classical model. This is due to the lower compressibility, the reduced density of states (see Sec. IV) and hence the lower electron concentration in the tip-induced band bending zone. Third, the current component arising from electrons tunneling out of the valence band (I_V, green dashed lines) is increased for the quantum corrected model, since the above discussed stronger screening of the tip-induced band bending leads to a larger number of valence band states available for tunneling. The enhanced screening is illustrated in Fig. 3(c), where the band edge positions vs distance are shown for a sample voltage of −1.5 V and under illumination. The enhanced screening reduces the band bending from the dashed white lines to the solid black line positions. As a result, the calculated total current $I_{total} = I_{Photo} + I_V$ is in very good agreement with the measurement for the quantum corrected simulation: in particular the match of the onset voltage, which is particularly important for the determination of the surface photovoltage, is improved significantly.

At last we compare the tunnel currents with [red solid line in Fig. 3(b)] and without [red dotted line in Fig. 3(a)] quantum correction using identical density of states (i.e., in parabolic band approximation). Deviations in the these two currents are caused by the quantum correction, only. Due to the above described occupation of the C_3 surface state and the resulting limitation of the band bending, the quantum correction alters the tunnel current in this special case by a factor of ≈2, only. However, this is still a significant change if quantitative physical parameters are determined by light excited STS. Without a surface state being occupied the effect is significantly larger as shown above for the case of GaN(10$\bar{1}$0).
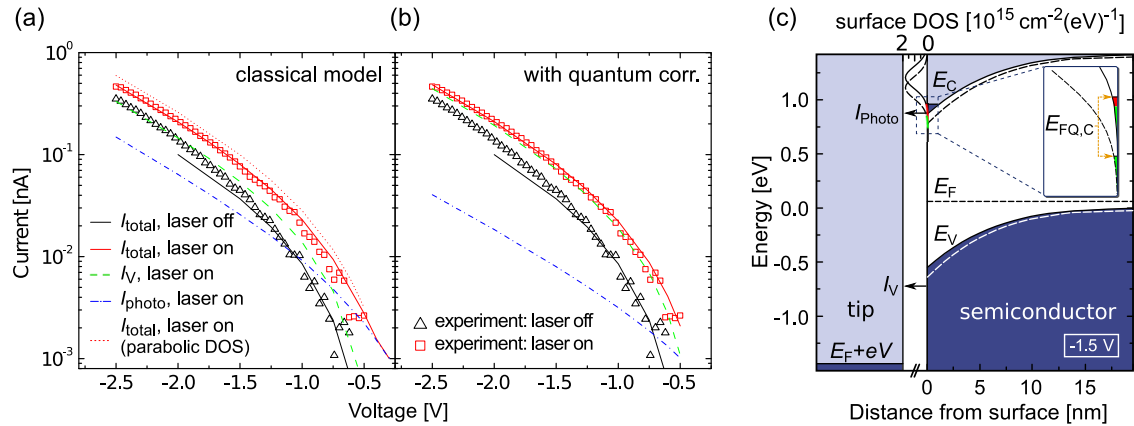
FIG. 3. Measured and simulated tunnel currents (a) without and (b) with incorporation of quantum compressibility for a GaAs(110) surface ([Zn] = $(1–2) \times 10^{18}$ cm^{-3}) at *negative* sample voltages. Besides the measured tunnel currents without (black triangles) and with (red squares) illumination, different simulated current contributions are plotted: the total current under dark conditions (black solid line), the current components arising from tunneling out of the valence band I_V (green dashed line) as well as out of the conduction band I_{Photo} (blue dash-dotted line) under illumination, and the total current under illumination (red solid line), which is the sum of the components I_V and I_{Photo}. It should be noted that no changes between the simulated currents with and without the incorporation of quantum compressibility occur at *positive* voltages due to the absence of regions with high carrier accumulation. For highlighting the effect of quantum compressibility only, compare the red solid line in (b) with the red dotted line in (a), which gives the simulated total current using the classical model with parabolic bands. (c) Band edge positions as a function of the distance from the surface of the semiconductor for a sample voltage of -1.5 V and under illumination. The dashed (solid) lines indicate the band edges for a simulation without (with) quantum correction. The upper scale shows the density of surface states C$_3$. Inset: magnification of the occupation of the Gaussian modeled C$_3$ surface state for the simulation with (solid line) and without (dashed line) quantum correction.

VI. CONCLUSIONS

Taking all the above aspects into consideration, the important role of quantum compressibility for the simulation of photoexcited scanning tunneling spectroscopy is evident: accurate determination of the carrier concentrations in the region of the tip-induced quantum dot cannot be achieved solely on the basis of classical semiconductor equations, since the drift and diffusion transport model requires adequate quantum correction. The introduction of an additional repulsive potential that accounts for quantum compressibility results in a significantly reduced carrier concentration near the semiconductor surface. As a result of the lower carrier concentration, it is sufficient to derive the corresponding quasi-Fermi energies within the parabolic band approximation, which improves the determination of the surface photovoltage. Hence the quantification of physical properties from photoexcited STS is improved strongly by including quantum correction. This correction must be applied not only for GaN(10$\bar{1}$0) or GaAs(110) but also for other materials and their nanostructures with higher carrier concentrations ($\gtrsim 1 \times 10^{18}$ cm^{-3}). Besides scanning tunneling microscopy and spectroscopy the formalism described above may improve other scanning probe related spectroscopy techniques.

[1] R. J. Hamers and K. Markert, Phys. Rev. Lett. **64**, 1051 (1990).

[2] Y. Kuk, R. S. Becker, P. J. Silverman, and G. P. Kochanski, Phys. Rev. Lett. **65**, 456 (1990).

[3] T. W. Matthes, C. Sommerhalter, A. Rettenberger, M. Böhmisch, J. Boneberg, M. C. Lux-Steiner, and P. Leiderer, Appl. Surf. Sci. **123-124**, 187 (1998).

[4] S. Aloni, I. Nevo, and G. Haase, Phys. Rev. B **60**, R2165(R) (1999).

[5] S. Aloni, I. Nevo, and G. Haase, J. Chem. Phys. **115**, 1875 (2001).

[6] S. Yoshida, Y. Kanitani, R. Oshima, Y. Okada, O. Takeuchi, and H. Shigekawa, Phys. Rev. Lett. **98**, 026802 (2007).

[7] S. Yoshida, Y. Kanitani, O. Takeuchi, and H. Shigekawa, Appl. Phys. Lett. **92**, 102105 (2008).

[8] S. Yoshida, Y. Kanitani, R. Oshima, Y. Okada, O. Takeuchi, and H. Shigekawa, Jpn. J. Appl. Phys. **47**, 6117 (2008).

[9] R. M. Feenstra, Surf. Sci. **603**, 2841 (2009).

[10] M. Schnedler, V. Portz, P. H. Weidlich, R. E. Dunin-Borkowski, and Ph. Ebert, Phys. Rev. B **91**, 235305 (2015).

[11] Y. Dong, R. M. Feenstra, R. Hey, and K. H. Ploog, J. Vac. Sci. Technol. B **20**, 1677 (2002).

[12] N. D. Jäger, Ph. Ebert, K. Urban, R. Krause-Rehberg, and E. R. Weber, Phys. Rev. B **65**, 195318 (2002).

[13] N. D. Jäger, E. R. Weber, K. Urban, and Ph. Ebert, Phys. Rev. B **67**, 165327 (2003).

[14] R. M. Feenstra, J. Y. Lee, M. H. Kang, G. Meyer, and K. H. Rieder, Phys. Rev. B **73**, 035310 (2006).

[15] S. Landrock, Y. Jiang, K. H. Wu, E. G. Wang, K. Urban, and Ph. Ebert, Appl. Phys. Lett. **95**, 072107 (2009).

[16] M. Schnedler, V. Portz, H. Eisele, R. E. Dunin-Borkowski, and P. Ebert, Phys. Rev. B **91**, 205309 (2015).

[17] D. L. Scharfetter and H. K. Gummel, IEEE Trans. Electron Devices **16**, 64 (1969).

[18] S. Selberherr, *Analysis and Simulation of Semiconductor Devices* (Springer, Vienna, 1984).

[19] F. Schwabl, *Statistical Mechanics*, 3rd ed. (Springer, Berlin, 2002).

[20] M. G. Ancona, J. Comput. Electron. **10**, 65 (2011).

[21] N. L. Rowsey and R. P. Muller, 3D TCAD Modeling of Candidate Structures for the Silicon Qubit, in *CSRI Summer Proceedings 2009*, edited by Z. Wen and S. S. Collis (Computer Science Research Institute at Sandia National Laboratories, Albuquerque, NM, 2010).

[22] A. Jüngel, *Quasi-Hydrodynamic Semiconductor Equations*, Progress in Nonlinear Differential Equations and Their Applications (Birkhäuser, Basel, 2011).

[23] C. de Falco, E. Gatti, A. L. Lacaita, and R. Sacco, J. Comput. Phys. **204**, 533 (2005).

[24] M. G. Ancona and H. F. Tiersten, Phys. Rev. B **35**, 7959 (1987).

[25] J. F. Creemer and P. J. French, *Ultra-thin Chip Technology and Applications* (Springer, New York, 2011), Chap. 22, pp. 271–286.

[26] M. R. Pinto, Ph.D. thesis, Stanford University, Dep. of Electrical Engineering, 1990.

[27] W. B. Joyce and R. W. Dixon, Appl. Phys. Lett. **31**, 354 (1977).

[28] J. R. Chelikowsky and M. L. Cohen, Phys. Rev. B **14**, 556 (1976).

[29] J. R. Chelikowsky and M. L. Cohen, Phys. Rev. B **30**, 4828 (1984).

[30] W. J. Yin, T. Shi, and Y. Yan, Adv. Mater. **26**, 4653 (2014).

[31] In Ref. [10] we modeled the probe tip as a hyperboloid and denoted the distance between the hyperboloid's focal point and it's vertex as the radius of the tip. Here, we use the more convenient radius of the osculating sphere as the tip radius. The actual shape of the tip that is used in the quantum corrected simulation is identical to the shape used in the classical simulation.

[32] N. Ishida, K. Sueoka, and R. M. Feenstra, Phys. Rev. B **80**, 075320 (2009).